ORIGINAL RESEARCH

Observation of different tumor motion magnitude within liver and estimate of internal motion margins in postoperative patients with hepatocellular carcinoma

Yu-Ting Zhao,[1,*] Zhi-Kai Liu,[2,*]
Qiu-Wen Wu,[3] Jian-Rong Dai,[1]
Tao Zhang,[1] Angela Y Jia,[4] Jing
Jin,[1] Shu-Lian Wang,[1] Ye-Xiong
Li,[1] Wei-Hu Wang[5]

[1]Department of Radiation Oncology,
National Cancer Center/Cancer Hospital,
Chinese Academy of Medical Sciences and
Peking Union Medical College, Beijing,
China; [2]Department of Radiation Oncology,
Peking Union Medical College Hospital,
Chinese Academy of Medical Sciences and
Peking Union Medical College, Beijing,
China; [3]Department of Radiation Oncology,
Duke University Medical Center, Durham,
NC, USA; [4]Department of Medicine,
Weill Cornell Medicine, New York, NY,
USA; [5]Key laboratory of Carcinogenesis
and Translational Research (Ministry of
Education/Beijing), Department of Radiation
Oncology, Peking University Cancer
Hospital and Institute, Beijing, China

*These authors contributed equally to this
work

Correspondence: Wei-Hu Wang
Key laboratory of Carcinogenesis
and Translational Research (Ministry
of Education/Beijing), Department of
Radiation Oncology, Peking University
Cancer Hospital and Institute, No 52
Fucheng Road, Haidian District, Beijing
100142, China
Tel +86 10 8819 6120
Fax +86 10 8819 6120
Email wangweihu88@163.com

Ye-Xiong Li
Department of Radiation Oncology,
National Cancer Center/Cancer Hospital,
Chinese Academy of Medical Sciences
and Peking Union Medical College, No 17
Panjiayuannanli, Chaoyang District, Beijing
100021, China
Email yexiong12@163.com

Aims: To assess motion magnitude in different parts of the liver through surgical clips in postoperative patients with hepatocellular carcinoma and to examine the correlation between the clip and diaphragm motion.

Methods: Four-dimensional computed tomography images from 30 liver cancer patients under thermoplastic mask immobilization were selected for this study. Three to seven surgical clips were placed in the resection cavity of each patient. The liver volume on computed tomography image was divided into the right upper (RU), right middle (RM), right lower (RL), hilar, and left lobes. Agreement between the clip and diaphragm motion was assessed by calculating intraclass correlation coefficient, and Bland–Altman analysis (*Diff*). Furthermore, population-based and patient-specific margins for internal motion were evaluated.

Results: The clips located in the RU lobe showed the largest motion, (7.5±1.6) mm, which was significantly more than in the RM lobe (5.7±2.8 mm, $p=0.019$), RL lobe (4.8±3.3 mm, $p=0.017$), and hilar lobe (4.7±2.7 mm, $p<0.001$) in the cranial–caudal direction. The mean intraclass correlation coefficient values between the clip and diaphragm motion were 0.915, 0.735, 0.678, 0.670, and the mean *Diff* values between them were 0.1±0.8 mm, 2.3±1.4 mm, 3.1±2.0 mm, 2.4±1.5 mm, when clips were located in the RU lobe, RM lobe, RL lobe, and hilar lobe, respectively. The clip and diaphragm motions had high concordance when clips were located in the RU lobe. Internal margin can be reduced from 5 mm in the cranial–caudal direction based on patient population average and to 3 mm based on patient-specific margins.

Conclusions: The motion magnitude of clips varied significantly depending on their location within the liver. The diaphragm was a more appropriate surrogate for tumor located in the RU lobe than for other lobes.

Keywords: hepatocellular carcinoma, surgical clips, diaphragm, motion magnitude, internal margin

Introduction

Liver cancer is the fifth most common malignancy and the third leading cause of cancer mortality worldwide.[1] Half of the cases and deaths are estimated to occur in China.[2] It is the fourth most frequently diagnosed cancer and the second leading cause of cancer mortality in China, where it accounts for 355,595 cases (10.54%) of all cancer, and results in 322,417 deaths annually.[3] Hepatocellular carcinoma (HCC) represents the major histological subtype of primary liver cancers, accounting for 70%–85% of the total liver cancer burden worldwide.[4]

Although HCC has been reported to be radiosensitive in clinical investigations,[5] the role of radiotherapy (RT) in the management of HCC was limited due to the poor tolerance of the whole liver to radiation.[6] Recently, to facilitate the partial liver irradiation, technologic advances such as intensity-modulated RT, proton RT, and carbon ion RT have been applied to HCC.[7–9] Moreover, potential reduction of radiation margins can be achieved through active breathing control, respiratory gating technique, or tumor tracking.[10–12] With the ability to facilitate escalation of the RT dose and minimize irradiation of normal tissue, the value of RT for HCC has been validated in recent years, and better survival has been achieved.[7–9,13–17]

The liver is difficult to immobilize and has been described as the "most moveable (abdominal) organ in both normal respiration and standardized breathing."[18] To apply these sophisticated RT technologies effectively, it is essential to understand and quantify target motion trajectories during treatment simulation and delivery, especially for patients who are unable to hold their breath for a long time during RT delivery. Several methods have been employed to measure the liver and liver tumor motions, including application of a scintillation camera after the administration of ^{99}Tc,[19,20] ultrasonography,[21] fluoroscopy,[22] computed tomography (CT),[23] cine-magnetic resonance imaging,[24] and electromagnetic transponders.[25,26] Respiratory-sorted "four-dimensional" CT (4DCT), one of the most commonly used imaging technologies, also has been applied to quantify the motion magnitude of liver and liver tumor during pretreatment simulation and fractionated treatment.[27–29] However, due to the poor image contrast, surrogates such as implanted metal markers, lipiodol, or diaphragm/liver contour are necessary.[28–30]

Various techniques suggested that the largest liver motion is usually observed in the cranial–caudal (CC) direction, with movements ranging widely from 5 to 50 mm.[18,21,25,26,31] Liver motion with the respiratory cycle is generally believed to be caused by the contraction and relaxation of the diaphragm. The motion must be considered in the radiation therapy treatment planning by adding margins to the planning target volume (PTV). Furthermore, the liver itself exhibits some deformation.[32] Therefore, we hypothesized that tumor displacement during the respiratory cycle depended on its location in the liver because the elasticity of the liver dampens the CC motion that is transmitted from the diaphragm and influenced by the traction of vessels. Although the diaphragm motion in the CC direction frequently serves as a breathing surrogate, it is uncertain whether this is reliable.[33] Yang et al[30] indicated that the concordance between tumor and diaphragm

motions changed according to the distance between the tumor and diaphragm. In this study, we employed 4DCT to measure the displacement of intrahepatic surgical clips as surrogate of the liver and the motion magnitude of the diaphragm in the setting of thermoplastic mask immobilization in postoperative patients with HCC, and then we examined the correlation of motion magnitude between the diaphragm and the clips implanted in the liver which is subdivided into five lobes.

Methods
Patients
In our hospital, the standard treatment protocol for patients with HCC adjacent to major vessels consists of intensity-modulated RT following narrow-margin hepatectomy. During surgery, the surgeons stitch radiopaque markers into the tumor bed for accurate localization of postoperative RT. The inclusion criteria for the protocol were as follows: 1) HCC without any adjuvant or neoadjuvant treatments except for postoperative RT; 2) radiopaque clips stitched around the tumor bed; 3) completion of training to achieve quiet and shallow breathing; 4) Child–Pugh Class A; 5) Eastern Cooperative Oncology Group Performance Status ≤1; and 6) no disease affecting cardiopulmonary function. Between May 2012 and December 2015, 30 postoperative patients (26 males, four females; median age: 54 year, range: 26–74 years) diagnosed with HCC were enrolled in this study. Institutional review board approval of Peking Union Medical College Hospital was obtained to retrospectively collect and study patient images, and the requirement for informed consent was waived because all images were already existing and all patient identification information had been removed.

4DCT data acquisition
The 4DCT images were acquired at least 3 weeks after surgery. Patients underwent scanning in the supine position on a 16-slice CT scanner (Brilliance 16; Philips Medical Systems, Cleveland, OH, USA) with the upper part of the body immobilized by a thermoplastic mask that was cut out from the xiphoid process to the umbilicus at the time of simulation.[15] The 4DCT imaging protocol was similar to that described previously by Pan et al.[34] Briefly, the scanner, connected to a respiration monitoring system (RPM; Varian Medical Systems, Palo Alto, CA, USA), was operated in cine-axial mode, with continuous scans performed at each CT couch location. Patients were instructed to breathe quietly during the scan, and 4DCT images were obtained only after a quiet and regular breathing pattern was observed. The scanning region extended from 4 cm above the top of the diaphragm

to the fourth lumbar vertebra, with a slice thickness of 3.0 mm; the resolution in the transverse plane was less than 1 mm in each direction. Based on the respiratory signal, the respiratory cycle was divided into 10 time-weighted phases that were defined as 0%–90%, which corresponded to the point in the respiratory cycle that the images represented. Typically, 0% represented the end-inhale phases and 50% represented the end-exhale. Then, the CT images of all phases were imported into the treatment planning system (Pinnacle[3] version 9.1; Philips Medical System, Madison, WI, USA).

Lobe definition

To test the hypothesis that tumor motions in various locations are different in the liver, the whole liver was divided into five lobes on the CT image according to the spatial relationship between anatomical structures (Figure 1). The part of the liver located on the left side of the falciform ligament was denoted as the left lobe, and the part located at 3 cm around the area where main hilar vessels enter the liver was classified as the hilar lobe. For the remaining part, a vertical line was drawn from the top of the right diaphragm to the lowest right edge on the coronal CT image. Then two transverse planes trisecting this vertical line were used to divide the remainder of the liver into three lobes, denoted as the right upper (RU) lobe, right middle (RM) lobe, and right lower (RL) lobe.

Structure delineation and motion measurement

For this study, the clips were initially automatically contoured in all phases on the axial CT slices by setting the auto-contouring threshold value between 800 and 1,200 (window 401, level 800 by Pinnacle); these contours were manually corrected afterward to remove the effect of imaging artifacts. A point of interest is defined to be at the centroid of the clip, ie, the center of the mass, and represents the clip for the subsequent motion analysis. The excursion of the clips from the 4DCT is thus obtained by calculating the difference between maximum and minimum of the 3D coordinates of these points of interest among 10 phases. Therefore, many systematic errors related to the CT images were canceled out, and the uncertainties should be, in general, less than the resolution of the CT images. It is difficult to automatically contour the liver and diaphragm directly. A single clinician contoured the regions of liver and diaphragm in all phases on the axial CT slices. The diaphragm contour was delineated by a 2 mm diameter circle at its most cranial part. A second clinician reviewed and approved all contours. Structure motion was defined as the excursion of the center of mass in the CC, anterior–posterior (AP), and left–right (LR) directions. Clip and whole liver displacements were measured in all three directions, while the diaphragm was measured only in the CC direction, given that only diaphragm motion in the CC direction was used as
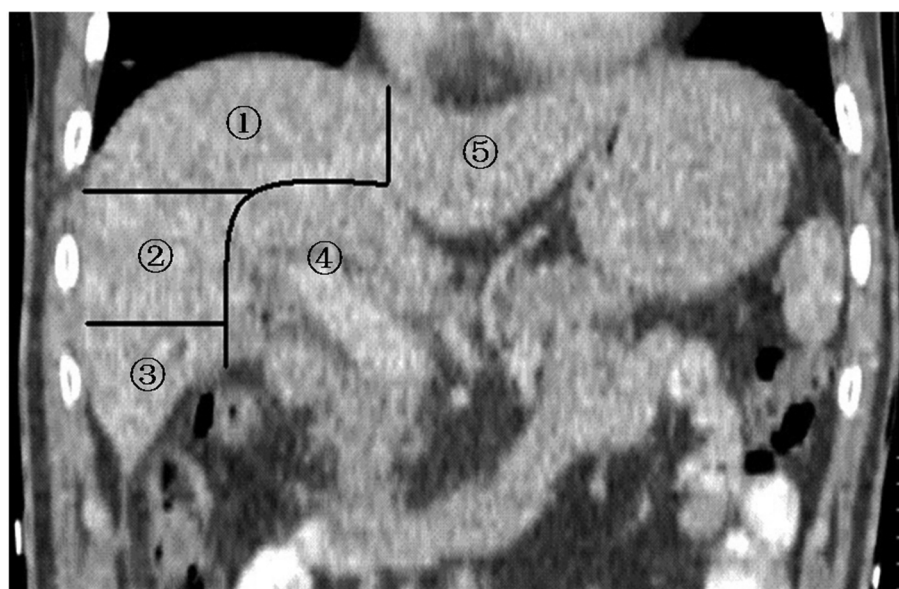

Figure 1 Coronal CT image of the five lobes of the liver.
Notes: ① RU lobe. ② RM lobe. ③ RL lobe. ④ Hilar lobe. ⑤ Left lobe.
Abbreviations: CT, computed tomography; RL, right lower; RM, right middle; RU, right upper.

a breathing surrogate in many previous studies and because it is also visually verifiable in fluoroscopy images at treatment simulation (conventional or CT simulator) and at treatment delivery (linac with on-board kV or MV imaging).

Location of clips

Three to seven radiopaque clips (titanium ring, diameter 4 mm) were placed in the resection cavity of each patient. Among 30 patients, a total of 125 radiopaque clips were placed around the tumor sites during surgery. Twenty-four clips were located in the RU lobe, 35 in the RM lobe, 19 in the RL lobe, 42 in the hilar lobe, and five in the left lobe (Figure 2). Given the low number of clips in the left lobe, this lobe was not included in subsequent analysis.

Statistical analysis

One-way analysis of variance was used for the analysis of statistical significance between the clip motions of different lobes. Agreement between the clip and diaphragm motions was assessed by calculating intraclass correlation coefficient (ICC) and Bland–Altman analysis. The ICC operated on data structured as groups, prohibiting outliers in the data groups from influencing the total correlation measured.[35] The higher ICC value indicated better correlation. However, ICC values alone were not sufficient to reflect good agreement between the clip and diaphragm motions because they only indicated the similar trend changing between two groups rather than providing a patient-by-patient comparison. The Bland–Altman analysis, a complementary measurement metric to better evaluate the agreement between the clip and diaphragm motions, calculated the difference of magnitudes (*Diff*) between the two motions on a point-by-point basis. A lower *Diff* indicated better correlation. Statistical significance was considered with p-value <0.05. One-way analysis of variance and ICC were carried out using SPSS version 19.0 statistical package (SPSS Inc., Chicago, IL, USA). Bland–Altman analysis (*Diff*) was performed using MedCalc for Windows, version 16.8.4 (MedCalc Software, Ostend, Belgium).

Internal margin estimate

When tumors in the thoracic and abdominal regions are considered for RT, the respiration motion-induced uncertainties must be evaluated during the treatment planning process. International Commission on Radiation Units and Measurements (ICRU) report 62 recommends that the margins for internal motion are explicitly included.[36] To estimate the magnitude of the internal margins for the liver tumor, several scenarios are considered based on the data collected and analyzed in this study. They are listed also in the order of how much motion information is available.

Population-based margin

In standard clinical practice, patients with HCC may only have free-breathing CT scan during simulation, and the motion of the tumor is unknown from the CT image. Therefore, the internal motion margin for a specific patient can
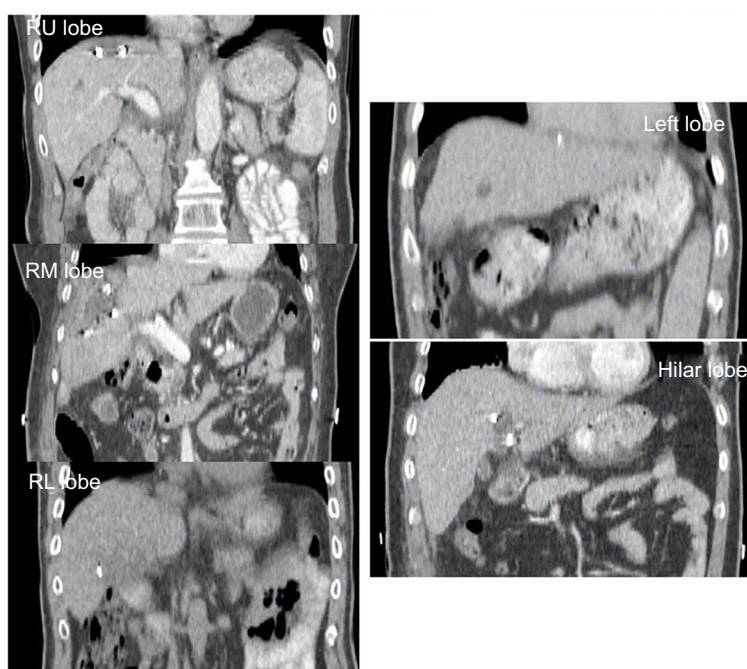

Figure 2 Examples of coronal CT images showing clips located in different lobes of the liver.
Abbreviations: CT, computed tomography; RL, right lower, RM, right middle; RU, right upper.

only be estimated from the population average, based on the data such as in this study. The same set of margin values are applied to all patients, although these margins may depend on which lobe of the liver the tumor resides. Also, different values may be applied for CC, AP, or LR directions. In our study, we calculated the population-based margins at 95% confidence level for tumors at each lobe. The values are based on the results in Table 1 and are given according to the formula: Margin = (Mean + 1.645 * SD)/2.0, for the 95% confidence level for one-tail normal distribution.

Patient-specific margin based on diaphragm motion

If some measurement is done on the diaphragm motion during the CT simulation, for example, fluoroscopy is performed to evaluate the excursion of the diaphragm, then it is reasonable to assume that this represents the maximum motion of the tumor in liver, regardless which lobe the tumor is in. Then, a patient-specific margin in the CC direction can be estimated in this way. However, one cannot infer the margins in other directions. To be conservative, one may use the same margin for other directions as well.

Patient-specific margin based on 4DCT

If 4DCT scan is performed for each patient at CT simulation, such as in those presented in this study, then more precise estimate can be made on the margins for the motion, which can be directly derived from the 4DCT. If the tumor borders multiple lobes with clips at more than one lobe, then only one lobe with the majority of the clips (≥2) is considered. For each patient, the margin was conservatively estimated using the maximum motion of all clips within the same lobe.

Results

Magnitude of motion

The mean magnitude of liver motion was (6.2±1.7) mm (range, 3.1–9.8) in the CC direction, (1.6±0.9) mm (range,

0.6–4.1) in the AP direction, and (2.1±1.2) mm (range, 0.4–5.0) in the LR direction. The greatest motion was observed in the CC direction. The mean motion magnitude of all clips was (5.6±2.8) mm (range, 0.5–11.2) in the CC direction, (1.6±1.3) mm (range, 0.4–6.5) in the AP direction, and (1.3±0.9) mm (range, 0.2–6.6) in the LR direction. Motions of clip (Mean ± SD) in different hepatic lobes in the CC, AP, and LR directions are shown in Table 1. The clips located in the RU lobe displayed the largest range of motion (7.5±1.6) mm in the CC direction, significantly more than those in either the RM lobe (5.7±2.8 mm; p=0.019), or the RL lobe (4.8±3.3 mm; p=0.017), or the hilar lobe (4.7±2.7 mm; p<0.001). The mean magnitude of diaphragm motion was (7.6±1.9) mm (range, 5.1–12.7) in the CC direction.

Correlation between clip motion and diaphragm motion

The mean values of ICC between the clip and diaphragm motions were 0.915, 0.735, 0.678, and 0.670 when clips were located in the RU lobe, RM lobe, RL lobe, and hilar lobe, respectively. Gradual decrease in ICC values was observed as the clip location varied in the CC direction, from the RU lobe, to the RM lobe, and to the RL lobe. The mean values of *Diff* between the clip and diaphragm motions were (0.1±0.8) mm, (2.3±1.4) mm, (3.1±2.0) mm, and (2.4±1.5) mm when clips were located in the RU lobe, RM lobe, RL lobe, and hilar lobe, respectively (Figure 3). The mean value of *Diff* was the smallest when the clips were located in the RU lobe. Therefore, the diaphragm motion agreed best with the clip motion when the clips were located in the RU lobe. These data demonstrated that the diaphragm would be a more reasonable direct surrogate for tumors located in the RU lobe.

Internal margin estimate

The population-based and patient-specific internal margins are listed in Table 2. They are calculated based on the values

Table 1 Motion magnitude (mean ± SD)

Location	Motion (mm)			Agreement with diaphragm	
	CC	**AP**	**LR**	**ICC**	**Bland–Altman (mm)**
Liver	6.2±1.7	1.6±0.9	2.1±1.2	–	–
Diaphragm	7.6±1.9	–	–	–	–
Clip					
All clips	5.6±2.8	1.6±1.3	1.3±0.9	–	–
RU lobe	7.5±1.6	3.0±2.0	2.2±1.0	0.915	0.1±0.8
RM lobe	5.7±2.8	1.6±1.1	1.1±1.1	0.735	2.3±1.4
RL lobe	4.8±3.3	1.1±0.4	1.2±0.7	0.678	3.1±2.0
Hilar lobe	4.7±2.7	0.9±0.6	1.0±0.5	0.670	2.4±1.5

Abbreviations: AP, anterior–posterior; CC, cranial–caudal; ICC, intraclass correlation coefficient; LR, left–right; RL, right lower, RM, right middle; RU, right upper; SD, standard deviation.
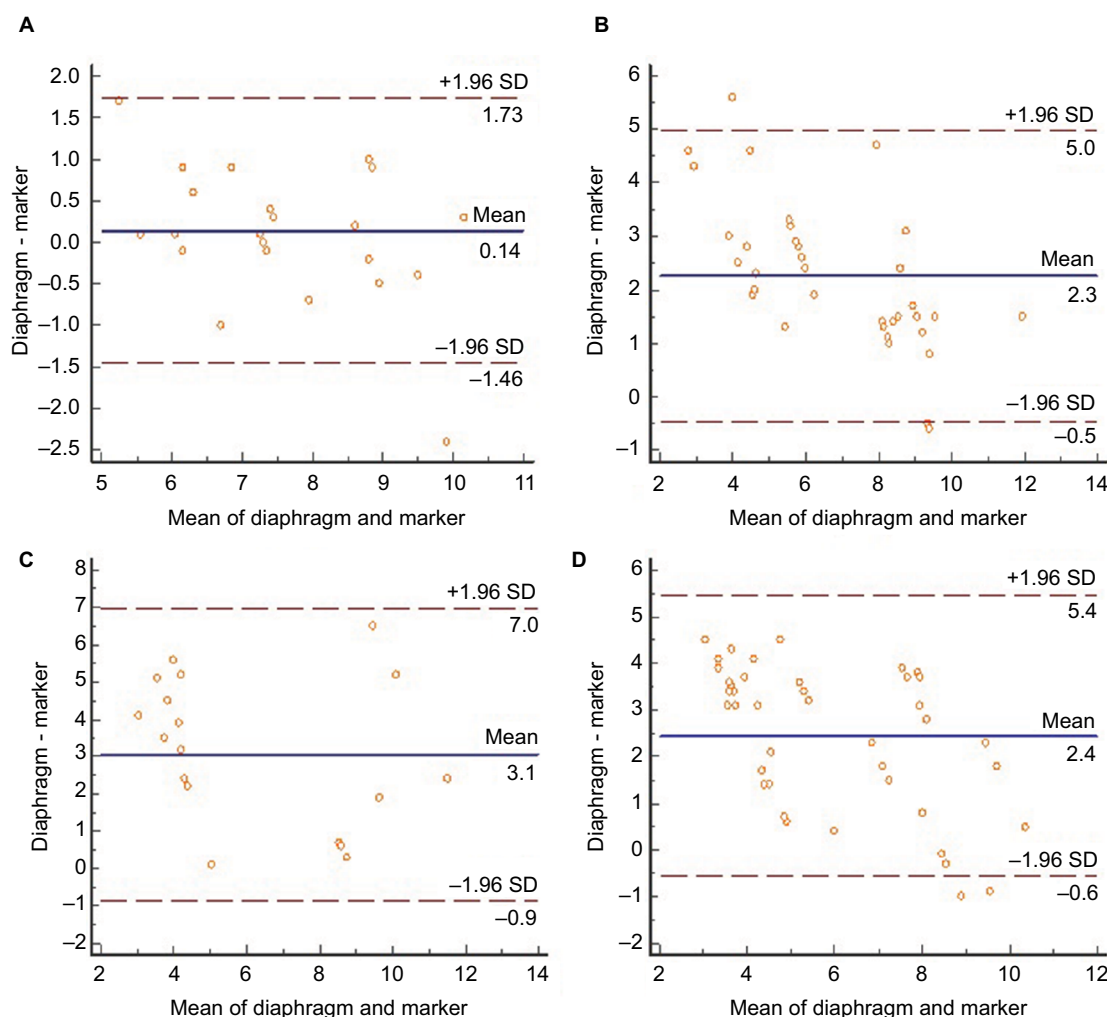
Figure 3 Bland–Altman analysis (*Diff*) for the clip and diaphragm motions in the CC direction, with clips located in the RU lobe (**A**), RM lobe (**B**), RL lobe (**C**), and hilar lobe (**D**).
Notes: The circles represent the difference in the motion magnitude between diaphragm and clip. The solid lines represent the mean values of *Diff*. The dotted lines represent the top and bottom 95% confidence interval values. Units in horizontal and vertical axes: mm.
Abbreviations: CC, cranial–caudal; RL, right lower; RM, right middle; RU, right upper.

Table 2 Population-based and patient-specific internal margin based on 4DCT for tumors in different lobes

Location	Population-based, mm			Patient-specific, mm		
	CC	AP	LR	CC	AP	LR
RU lobe	5.1	3.1	1.9	4.1±1.0	1.9±1.3	1.4±0.5
RM lobe	5.2	1.7	1.4	3.1±1.8	1.2±0.8	0.6±0.3
RL lobe	5.1	0.9	1.1	3.1±2.0	0.7±0.2	0.7±0.4
Hilar lobe	4.6	0.9	0.9	2.7±1.4	0.6±0.2	0.7±0.2

Abbreviations: 4DCT, Four-dimensional computed tomography; AP, anterior–posterior; CC, cranial–caudal; LR, left–right; RL, right lower, RM, right middle; RU, right upper.

given in Table 1 with 95% confidence level. The margin values in the CC direction are – as expected – much larger than in the other two directions, and therefore it is the dominant one. It is interesting to note that the CC margin is almost independent of the lobes, even though the motion magnitudes at each lobe are significantly different, as shown

previously. This is because the standard deviations of the marker motion are significantly different from lobe to lobe and the margin values are the combination of the mean value and the standard deviation.

Patient-specific margin based on the diaphragm motion is simply ½ of the diaphragm motion, ie, (3.8±1.0) mm. While

this number may appear comparable to the population-based one, it is different for each patient.

To derive the patient-specific margins based on the 4DCT data, data for each patient are examined. Overall, the number of patients having tumor in the RU lobe, RM lobe, RL lobe, and hilar lobe are six, seven, four, and 11 respectively. Two patients with no dominant lobe were excluded from this analysis. The trend is that, as expected, the margin is getting smaller with increasing distance between the lobe and the diaphragm.

It is worth pointing out that the population-based margins in Table 2 apply to all patients, while the patient-specific margins are the average from 30 patients, and therefore their standard deviations are also listed.

Discussion

In this study, we implanted radiopaque clips around tumor sites to monitor the respiratory clip motion by using 4DCT in postoperative patients with HCC. To our knowledge, this study is the first to assess motion magnitude of the liver, intrahepatic clips, and diaphragm in the setting of thermoplastic mask immobilization in postoperative patients. We also pioneered subdividing the liver according to a five-lobe classification scheme to investigate the relationship between the intrahepatic clips of individual lobes and diaphragm motions. We observed that the clips located in various lobes within the liver have different motion magnitudes. Specifically, clips located in the RU lobe, which were in close proximity to the diaphragm, exhibited a larger motion than the other lobes. We find that the diaphragm motion agreed best with the clip motion when the clips were located in the RU lobe, a confirmation of results of previous studies such as that by Yang et al.[30]

The mean motion magnitudes of liver and clips from our study were slightly smaller than previous studies.[28,37] Case et al[37] reported the mean liver motion amplitude for patients treated during free breathing was 8.0 mm (range, 0.1–18.8), 4.3 mm (range, 0.1–12.1), and 1.8 mm (range, 0.1–7.0) in the CC, AP, and LR directions, respectively. Beddar et al[28] analyzed the internal fiducial motion for liver tumors imaged with 4DCT. The results showed that the range of motion of the fiducials was 7.5–17.5 mm, 1.2–8.7 mm, and 1.1–5.0 mm in the CC, AP, and LR directions, respectively. The difference may be partially explained by the fact that the patients in our study were immobilized with a thermoplastic mask and patients were instructed to perform quiet and shallow breathing. The thermoplastic mask, to a certain extent, has the effect of abdominal compression and induces high-frequency ventilation which can reduce respiratory mobility. A preclinical

animal study indicated that the use of high-frequency jet ventilation would be able to limit the liver motion to an extent acceptable for the application of radiosurgery in humans.[38] Furthermore, the motion magnitude of patients who had received partial hepatectomy was significantly smaller than that of patients who had no history of any hepatic surgical procedures.[39] The derived internal margins are only valid for this patient cohort.

Moreover, we found that the clips located in various lobes within the liver have different motion magnitudes that decrease in the CC direction. The RU lobe, likely due to its proximity to the diaphragm, demonstrated the greatest range of motion. Our results were consistent with previous studies of lung cancer patients where tumors located in the lower lobes of the lungs exhibited a greater degree of motion than those located in the superior lung lobes, and that such motion mainly occurred along the CC dimension.[40–43] For example, Redmond et al[40] found that the mean CC excursion was 9.0 mm in lower-lobe tumors versus 4.3 mm in upper-lobe tumors ($p=0.011$). Furthermore, Pantarotto et al[44] analyzed the motion of 100 mediastinal lymph nodes from 41 patients with lung cancer and reported that the magnitude of nodal motion was significantly greater for nodes closer to the diaphragm. The lower mediastinal nodes had the greatest degree of motion (mean, 0.79 cm), significantly more than those in either the upper (mean, 0.53 cm; $p=0.001$) or middle mediastinum (mean, 0.68 cm; $p=0.007$).

The diaphragm is frequently used as a surrogate in the CC direction, because the tumor contrast within the liver is often too low for direct target localization. However, Kirilova et al[24] demonstrated that liver tumor motion did not correlate well with the diaphragm motion ($r=0.25$). Seppenwoolde et al[45] indicated that some situations demand considerable margin to account for the uncertainty in the correlation between the diaphragm dome and the tumor. Chan et al[29] suggested that the margin required for the tumor prediction error using the diaphragm surrogate was 11.7 mm in the CC direction. Paganelli et al[33] determined that the surrogate-based tracking errors (relative to the motion amplitude) were in the range of 7%–23% (1.02–3.57 mm). Yang et al[30] indicated that tumor and diaphragm motions had high concordance when the distance between the tumor and tracked diaphragm area was small. In order to further investigate this issue, we divided the whole liver into five lobes and compared each lobe with the diaphragm. Our results indicated that using the diaphragm as a surrogate for target motion magnitude depends predominantly on the location of the primary tumor. The diaphragm was a more reasonable surrogate when the

tumor was located in the RU lobe. Increased margins would be added to PTV if the diaphragm was used as a surrogate for tumor in the RM lobe, RL lobe, and hilar lobe, resulting in irradiation of a larger volume of healthy tissue than necessary, which increases the risk of normal tissue toxicity.

Margin evaluations in this study were limited at the geometrical scope, and more comprehensive dosimetric analysis may be necessary to provide more insight. Also, the margins discussed only represent the internal margin. In practice, other margins such as setup errors, deformations, baseline shifts, and inter-fractional motion variability should also be included in the PTV. Nevertheless, some useful information can be obtained from these simple analyses. One take home message is that, compared to the population-based margin, about 5 mm in CC direction, the patient-specific margins are more accurate and preferred, and in general, they are smaller, too. They are approximately 4 mm in CC when based on diaphragm motion, and 3 mm to 4 mm when based on 4DCT. The finding that the patient-specific margin is smaller than population-based margin is not surprising and is consistent with previous investigations for other sites such as in prostate cancer. This reassures the belief that as more advanced technology is used during the CT simulation of liver cancer patients, more information about the tumor motion can be obtained and the patient-specific margins can thus be reduced, which can potentially reduce the RT toxicity and allow escalation of the prescription dose. This will help move toward individualized patient treatment planning and implementation of precision medicine. Furthermore, if additional measures are taken during treatment delivery, such as implementation of respiratory-gated delivery or motion-synchronized delivery, the internal margin can be further reduced.

There are a number of limitations in this report. First of all, our data are representative of only the postoperative patients with HCC. The surgery may alter the liver elasticity and its ability to deform due to the respiration. Therefore, this group of patients may not be representative of the majority who underwent RT with large and inoperable intrahepatic tumors in current practice. Second, liver deformation with respiration affects the whole liver volume, but only a few sparsely located landmarks (clips) were used in this study, which may not be representative of the whole liver volume behavior, although with less uncertainties in identification. Third, 4DCT at simulation cannot accurately predict the daily tumor motion, compared with cone-beam CT.[46,47] Limitations of 4DCT in detecting the liver motion, such as in the limited breathing cycles and the different breathing patterns between CT simulation and treatment may need additional margins to account for these uncertainties. 4D magnetic resonance imaging is an emerging technology that is potentially more accurate than 4DCT in characterizing the liver motion during treatment.[48–50] However, it is not yet mature enough for routine clinical use. Finally, our cohort was not large enough to allow a more meaningful location subtype analysis, especially with only five clips in the left lobe. Therefore, all findings require validation with larger patient numbers.

Conclusion

In conclusion, the motion magnitude of the clips differed based on clip location in the liver in postoperative patients with HCC. Clips located in the RU lobe displayed a greater range of motion in the CC direction than clips located in other lobes. This finding suggests that site-specific PTV margins are required for different tumor locations in the liver. For patients with multiple lesions at various locations, different margins may be necessary. In addition, the diaphragm was a more appropriate surrogate for tumors in the RU lobe than for those in the other lobes. Internal margins accounting for the respiratory motion can be reduced when additional motion measurements are performed, such as the diaphragm motion and 4DCT scan during CT simulation.

Acknowledgments

Disclosure

The authors report no conflicts of interest in this work.

References

1. Jemal A, Bray F, Center MM, Ferlay J, Ward E, Forman D. Global cancer statistics. *CA Cancer J Clin.* 2011;61(2):69–90.
2. Ferlay J, Shin HR, Bray F, Forman D, Mathers C, Parkin DM. Estimates of worldwide burden of cancer in 2008: GLOBOCAN 2008. *Int J Cancer*. 2010;127(12):2893–2917.
3. Chen W, Zheng R, Zeng H, Zhang S, He J. Annual report on status of cancer in China, 2011.*Chin J Cancer Res*. 2015;27(1):2–12.
4. Perz JF, Armstrong GL, Farrington LA, Hutin YJ, Bell BP. The contributions of hepatitis B virus and hepatitis C virus infections to cirrhosis and primary liver cancer worldwide. *J Hepatol*. 2006;45(4):529–538.
5. Seong J, Park HC, Han KH, Chon CY. Clinical results and prognostic factors in radiotherapy for unresectable hepatocellular carcinoma: a retrospective study of 158 patients. *Int J Radiat Oncol Biol Phys.* 2003;55(2):329–336.
6. Stillwagon GB, Order SE, Guse C, et al. 194 hepatocellular cancers treated by radiation and chemotherapy combinations: toxicity and response: a Radiation Therapy Oncology Group Study. *Int J Radiat Oncol Biol Phys.* 1989;17(6):1223–1229.
7. Hawkins MA, Dawson LA. Radiation therapy for hepatocellular carcinoma: from palliation to cure. *Cancer*. 2006;106(8):1653–1663.

8. Fukumitsu N, Sugahara S, Nakayama H, et al. A prospective study of hypofractionated proton beam therapy for patients with hepatocellular carcinoma. *Int J Radiat Oncol Biol Phys*. 2009;74(3):831–836.

9. Kato H, Tsujii H, Miyamoto T, et al. Results of the first prospective study of carbon ion radiotherapy for hepatocellular carcinoma with liver cirrhosis. *Int J Radiat Oncol Biol Phys*. 2004;59(5):1468–1476.

10. Eccles C, Brock KK, Bissonnette JP, Hawkins M, Dawson LA. Reproducibility of liver position using active breathing coordinator for liver cancer radiotherapy. *Int J Radiat Oncol Biol Phys*. 2006;64(3):751–759.

11. Ge J, Santanam L, Yang D, Parikh PJ. Accuracy and consistency of respiratory gating in abdominal cancer patients. *Int J Radiat Oncol Biol Phys*. 2013;85(3):854–861.

12. Sothmann T, Blanck O, Poels K, Werner R, Gauer T. Real time tracking in liver SBRT: comparison of CyberKnife and Vero by planning structure-based γ-evaluation and dose-area-histograms. *Phys Med Biol*. 2016;61(4):1677–1691.

13. Bujold A, Massey CA, Kim JJ, et al. Sequential phase I and II trials of stereotactic body radiotherapy for locally advanced hepatocellular carcinoma. *J Clin Oncol*. 2013;31(13):1631–1639.

14. Huo YR, Eslick GD. Transcatheter arterial chemoembolization plus radiotherapy compared with chemoembolization alone for hepatocellular carcinoma: a systematic review and Meta-analysis. *JAMA Oncol*. 2015;1(6):756–765.

15. Wang WH, Wang Z, Wu JX, et al. Survival benefit with IMRT following narrow-margin hepatectomy in patients with hepatocellular carcinoma close to major vessels. *Liver Int*. 2015;35(12):2603–2610.

16. Wahl DR, Stenmark MH, Tao Y, Pollom EL, Caoili EM, Lawrence TS, et al. Outcomes after stereotactic body radiotherapy or radio-frequency ablation for hepatocellular carcinoma. *J Clin Oncol*. 2016;34(5):452-459.

17. Zhang T, Zhao YT, Wang Z, et al. Efficacy and safety of intensity-modulated radiotherapy following transarterial chemoembolization in patients with unresectable hepatocellular carcinoma. *Medicine (Baltimore)*. 2016;95(21):e3789.

18. Suramo I, Paivansalo M, Myllyla V. Cranio-caudal movements of the liver, pancreas and kidneys in respiration. *Acta Radiol Diagn*. 1984;25(2):129–131.

19. Weiss PH, Baker JM, Potchen EJ. Assessment of hepatic respiratory excursion. *J Nucl Med*. 1972;13(10):758–759.

20. Harauz G, Bronskill MJ. Comparison of the liver's respiratory motion in the supine and upright positions: Concise communication. *J Nucl Med*. 1979;20(7):733–735.

21. Davies SC, Hill AL, Holmes RB, Halliwell M, Jackson PC. Ultrasound quantitation of respiratory organ motion in the upper abdomen. *Br J Radiol*.1994;67(803):1096–1102.

22. Gierga DP, Chen GTY, Kung JH, Betke M, Lombardi J, Willett CG. Quantification of respiration-induced abdominal tumor motion and its impact on IMRT dose distributions. *Int J Radiat Oncol Biol Phys*. 2004;58(5):1584–1595.

23. Balter JM, Lam KL, McGinn CJ, Lawrence TS, Ten Haken RK. Improvement of CT based treatment-planning models of abdominal targets using static exhale imaging. *Int J Radiat Oncol Biol Phys*. 1998;41(4):939–943.

24. Kirilova A, Lockwood G, Choi P, et al. Three-dimensional motion of liver tumors using cine-magnetic resonance imaging. *Int J Radiat Oncol Biol Phys*. 2008;71(4):1189–1195.

25. Poulsen PR, Worm ES, Hansen R, et al. Respiratory gating based on internal electromagnetic motion monitoring during stereotactic liver radiation therapy: First results. *Acta Oncol*. 2015;54(9):1445–1452.

26. Habermehl D, Naumann P, Bendl R, et al. Evaluation of inter-and intrafractional motion of liver tumors using interstitial markers and implantable electromagnetic radiotransmitters in the context of image-guided radiotherapy (IGRT)-the ESMERALDA trial. *Radiat Oncol*. 2015;14(10):143.

27. Brandner ED, Wu A, Chen H, et al. Abdominal organ motion measured using 4D CT. *Int J Radiat Oncol Biol Phys*. 2006;65(2):554–560.

28. Beddar AS, Kainz K, Briere TM, et al. Correlation between internal fiducial tumor motion and external marker motion for liver tumors imaged with 4D-CT. *Int J Radiat Oncol Biol Phys*. 2007;67(2):630–638.

29. Chan MK, Lee V, Chiang CL, et al. Lipiodol versus diaphragm in 4D-CBCT-guided stereotactic radiotherapy of hepatocellular carcinomas. *Strahlenther Onkol*. 2016;192(2):92–101.

30. Yang J, Cai J, Wang H, et al. Is diaphragm motion a good surrogate for liver tumor motion? *Int J Radiat Oncol Biol Phys*. 2014;90(4):952–958.

31. Balter JM, Dawson LA, Kazanjian S, et al. Determination of ventilatory liver movement via radiographic evaluation of diaphragm position. *Int J Radiat Oncol Biol Phys*. 2001;51(1):267–270.

32. Miller K. Constitutive modeling of abdominal organs. *J Biomech*. 2000;22:367–373.

33. Paganelli C, Seregni M, Fattori G, et al. Magnetic resonance imaging-guided versus surrogate-based motion tracking in liver radiation therapy: a prospective comparative study. *Int J Radiation Oncol Biol Phys*. 2015;91(4):840–848.

34. Pan T, Lee TY, Rietzel E, Chen GT. 4D-CT imaging of a volume influenced by respiratory motion on multi-slice CT. *Med Phys*. 2004;31(2):333–340.

35. Weir JP. Quantifying test-retest reliability using the intraclass correlation coefficient and the SEM. *J Strength Cond Res*. 2005;19(1):231–240.

36. International Commission on Radiation Units and Measurements. Prescribing, recording, and reporting photon beam therapy (supplement to ICRU report 50). ICRU report 62. Bethesda, MD: ICRU; 1999.

37. Case RB, Sonke JJ, Moseley DJ, et al. Interfraction and intrafraction changes in amplitude of breathing motion in stereotactic liver radiotherapy. *Int J Radiat Oncol Biol Phys*. 2010;77(3):918–925.

38. Yin FF, Kim JG, Haughton C, et al. Extracranial radiosurgery: Immobilizing liver motion in dogs using high-frequency jet ventilation and total intravenous anesthesia. *Int J Radiat Oncol Biol Phys*. 2001;49(1):211–216.

39. Kitamura K, Shirato H, Seppenwoolde Y, et al. Tumor location, cirrhosis, and surgical history contribute to tumor movement in the liver, as measured during stereotactic irradiation using a real-time tumor-tracking radiotherapy system. *Int J Radiat Oncol Biol Phys*. 2003;56(1):221–228.

40. Redmond KJ, Song DY, Fox JL, Zhou J, Rosenzweig CN, Ford E. Respiratory motion changes of lung tumors over the course of radiation therapy based on respiration-correlated four-dimensional computed tomography scans. *Int J Radiat Oncol Biol Phys*. 2009;75(5):1605–1612.

41. Liu HH, Balter P, Tutt T, et al. Assessing respiration-induced tumor motion and internal target volume using four-dimensional computed tomography for radiotherapy of lung cancer. *Int J Radiat Oncol Biol Phys*. 2007;68(2):531–540.

42. Onimaru R, Shirato H, Fujino M, et al. The effect of tumor location and respiratory function on tumor movement estimated by real-time tracking radiotherapy (RTRT) system. *Int J Radiat Oncol Biol Phys*. 2005;63(1):164–169.

43. Seppenwoolde Y, Shirato H, Kitamura K, et al. Precise and real-time measurement of 3D tumor motion in lung due to breathing and heart-beat, measured during radiotherapy. *Int J Radiat Oncol Biol Phys*. 2002;53(4):822–834.

44. Pantarotto JR, Piet AH, Vincent A, van Sörnsen de Koste JR, Senan S. Motion analysis of 100 mediastinal lymph nodes: potential pitfalls in treatment planning and adaptive strategies. *Int J Radiat Oncol Biol Phys*. 2009;74(4):1092–1099.

45. Seppenwoolde Y, Wunderink W, Wunderink-van Veen SR, Storchi P, Méndez Romero A, Heijmen BJ. Treatment precision of image-guided liver SBRT using implanted fiducial markers depends on marker-tumour distance. *Phys Med Biol*. 2011;56(17):5445–5468.

46. Rankine L, Wan H, Parikh P, et al. Cone-beam computed tomography internal motion tracking should be used to validate 4-dimensional computed tomography for abdominal radiotherapy patients. *Int J Radiat Oncol Biol Phys*. 2016;95(2):818–826.

47. Worm ES, Hoyer M, Fledelius W, Hansen AT, Poulsen PR. Variations in magnitude and directionality of respiratory target motion throughout full treatment courses of stereotactic body radiotherapy for tumors in the liver. *Acta Oncol*. 2013;52(7):1437–1444.

48. Cai J, Chang Z, Wang Z, Paul Segars W, Yin FF. Four-dimensional magnetic resonance imaging (4D-MRI) using image-based respiratory surrogate: a feasibility study. *Med Phys*. 2011;38(12):6384–6394.

49. Paganelli C, Summers P, Bellomi M, Baroni G, Riboldi M. Liver 4DMRI: A retrospective image-based sorting method. *Med Phys*. 2015;42(8):4814–4821.

50. Brix L, Ringgaard S, Sorensen TS, Poulsen PR. Three-dimensional liver motion tracking using real-time two-dimensional MRI. *Med Phys*. 2014;41(4):042302.